Thermal Science and Engineering Progress 8 (2018) 296–306

Contents lists available at ScienceDirect

Thermal Science and Engineering Progress

journal homepage: www.elsevier.com/locate/tsep

Performance of evacuated flat plate solar thermal collectors

Roger Moss[a,*], Stan Shire[a], Paul Henshall[b], Farid Arya[c], Philip Eames[d], Trevor Hyde[c]

[a] School of Engineering, University of Warwick, Coventry, UK
[b] Oxford Brookes University, formerly CREST, Loughborough University, Loughborough, UK
[c] School of the Built Environment, University of Ulster, Belfast, UK
[d] Centre for Renewable Energy Systems Technology, Loughborough University, UK

ARTICLE INFO

Keywords:
Solar thermal
Flat plate
Vacuum
Evacuated
Uncertainty

ABSTRACT

Heat losses from a flat panel solar collector can be significantly reduced by lowering the internal pressure to < 0.5 Pa. Compared with conventional collectors, the resulting increase in efficiency is predicted to give a significant gain in annual heat output in the context of a temperate climate with low median irradiance.

Two experimental collectors were built and tested to investigate theoretical aspects of evacuated flat plates and develop appropriate technological solutions. One had a metal tray to the rear, the other used two sheets of glass. An array of pillars supports the glass against atmospheric pressure. The experimental procedure was designed to minimise measurement uncertainty. Testing under a solar simulator, with and without a vacuum, showed a sudden drop in heat loss as the pressure was reduced below 0.5 Pa. When evacuated the heat loss coefficient fell from 7.43 to 3.65 $W/m^2 K$ and the efficiency at a nominal test condition of $\Delta T = 60\,^{\circ}C$, $G = 1000\ W/m^2$ increased from 36% to 56%. Heat losses from absorber to glass were within 9% of the predicted level. This demonstrates that the heat loss mechanism is well understood.

1. Introduction

The research programme summarised in this paper was a collaboration between the University of Warwick, Loughborough University and Ulster University. It aimed to deepen the theoretical understanding of stresses in vacuum enclosures, develop practical techniques for their fabrication, demonstrate the performance benefits and disseminate the resulting knowledge. Two evacuated flat panel collectors were built and tested under a solar simulator.

The production of low temperature heat accounts for 47% of fossil fuel consumption and 25% of carbon dioxide emissions in the UK. Given suitable weather, solar thermal collectors can play a part in satisfying this demand. Solar collector efficiency falls as the fluid to ambient temperature difference increases and/or as illumination levels decrease: the highest possible efficiency is desirable if the collector is intended for use in cold conditions, on overcast days or with high delivery temperatures.

There have been many attempts over the past 40 years to improve solar collector efficiency; recent developments are summarised by Suman [1]. Some reduction in heat loss is possible by reducing the internal pressure to inhibit convection (Benz [2], Beikircher [3]): this is feasible without great expense. At moderate pressures the conduction loss is not eliminated, though in the absence of convection an increased gap may be used to reduce heat losses.

The efficiency of a solar thermal collector can be increased even further if the internal pressure is reduced until the molecular mean free path exceeds the distance between absorber and cover glass. A pressure of order 0.5 Pa or less is required. Conduction is then eliminated and the only heat loss mechanism is by radiation.

This principle is commonly used in evacuated tube solar collectors. Its extension to flat plate collectors can achieve a higher fill factor and be more architecturally attractive. An evacuated flat panel could also be useful as a thermally insulating building component, for instance in building façades.

Fig. 1 shows published efficiency curves at $G = 1000\ W/m^2$ for a variety of solar collector architectures.

The best optical efficiency (y-intercept) is obtained by flat plate collectors (FP); the heat loss coefficient U_L (line gradient) can be somewhat reduced using a double glazed cover (FP (double glazed)). Evacuated tubes (ET, ET + reflector) typically have lower heat loss coefficients but lower optical efficiency since the tube internal diameter which limits the absorber strip width is necessarily less than the outer diameter and tube spacing.

Another approach to improving high temperature efficiency is to use a concentrating collector (Buttinger [6], Cohen [7], Zou [8]). Parabolic trough collectors (PTC) for instance achieve very low heat

* Corresponding author.
E-mail address: r.moss@warwick.ac.uk (R. Moss).

https://doi.org/10.1016/j.tsep.2018.09.003
Received 6 April 2018; Received in revised form 13 July 2018; Accepted 8 September 2018

Nomenclature

G	total (beam + diffuse) irradiance (W/m^2) measured perpendicular to collector
T_a	ambient temperature (°C)
T_{env}	environment radiative (sky) temperature (°C)
T_g	cover glass temperature (°C)
T_p	plate mean surface temperature (°C)
T_M	mean temperature difference $T_p - T_a$(°C)
U_L	overall heat loss coefficient (W/m^2 K)
f_b, f_d	beam and diffuse fractions of the aperture-normal radiation
h_i, h_o	heat transfer coefficient (W/m^2 K) to inward or outward-facing glass surface
q_{abs}	Rate of heat absorption in glass (W/m^2)
α	coating absorptivity
ε	emissivity
ε_{eg},ε_{pg}	effective emissivity, environment to glass, plate to glass
η	efficiency (absorber and gross area definition as appropriate)
η_o	optical efficiency
η_{ob}, η_{od}	beam and diffuse optical efficiency components for a trough collector
σ	Stefan-Boltzmann constant

loss coefficients at the expense of optical efficiency; the need for tracking to follow the Sun's position tends to make such designs unsuitable for mounting on buildings. Two optical efficiency constants are required because the trough focusses beam radiation but only captures a small fraction of the diffuse illumination:

$$\eta = f_b \eta_{ob} + f_d \eta_{od} - \frac{U_L T_M}{G} \quad (1)$$

Curve fits to SPF data for the NEP PolyTrough 1800 suggest $\eta_{ob} = 0.689$, $\eta_{od} = 0.096$ and $U_L = 0.36 + 0.0011 T_M$ W/m^2 K (based on aperture area) for a typical concentrating trough collector. Parabolic trough collectors are suitable for generating high temperature steam for use in a Rankine cycle (Bouvier, [9]); the poor diffuse-light efficiency limits the usefulness of such collectors in a temperate climate.

Where high temperatures are not required, the evacuated flat plate concept is generally more attractive than concentrating collectors because it has good diffuse-light efficiency and does not require tracking.

TVP Solar [10] manufacture evacuated flat collectors for industrial process heat applications. SRB also used to produce evacuated panels (Benvenuti [11–13]) but appear to have ceased trading.

Many of the proprietary construction details of the TVP and SRB panels are unpublished: this paper aims to remedy that situation. TVP supply collectors for solar fields > 500 m^2. The possibility of obtaining one to include in the project tests was not considered as it seemed unlikely that this would lead to significant technical insights: the purpose of the research was to thoroughly investigate theoretical and manufacturing aspects of evacuated collector design rather than simply duplicate commercial performance data.

For reference purposes, Fig. 1 includes published data for two SRB panels. The SRB C0 was a stand-alone model whilst the SRB C1 included side reflectors that reflect light onto the underside of the absorber, effectively giving a slight concentration effect (reduced efficiency gradient) but with a lower optical efficiency in terms of gross area. It seems probable that the evacuated collector unit was relatively expensive: the mirrors would then be a cost-effective means of increasing the output.

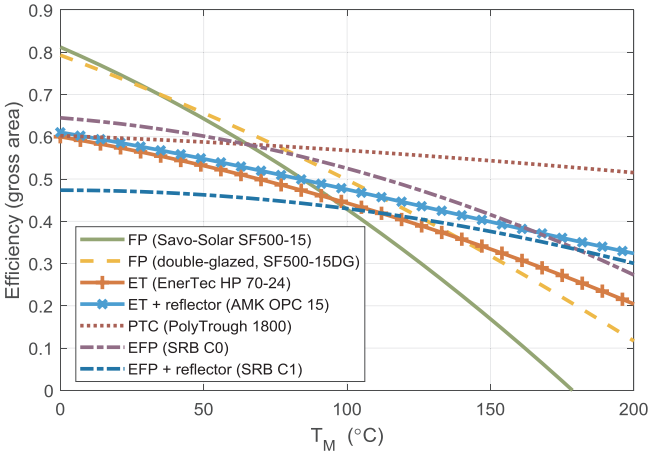

Fig. 1. Comparison of published data for solar collector architectures at G_b = 1000 W/m^2. (SPF catalogue [4]; SRB curves from Pauletta [5]).

2. Design and manufacture

2.1. Absorber design

The absorber plate used a flooded design made by hydroforming and TIG welding 0.7 mm sheets of 316 L stainless steel; a pressure of 19.3 MPa was used (Figs. 2 and 3). A flooded design provides the low pumping power benefits of a micro-channel plate (Moss, [14]) but is easier to fabricate. The intention was to achieve a high collector efficiency factor despite the relatively poor conductivity of stainless steel, Moss [15].

The hydroforming mould created an array of dimples. After cutting and welding, these formed an array of holes at 60 mm pitch through which the 6 mm diameter support pillars could pass. There is no contact between the pillars and absorber: this is necessary to avoid a conduction path to the cover glass. Flow uniformity was assessed in Star-CCM +. The material thickness was chosen following a stress analysis in Abaqus CAE (Moss, [15]).

Black chrome plating was used as a spectrally selective absorbing coating: whilst not as selective as proprietary mass-produced coatings, it was available locally for one-off applications. The undesirably high emissivity obtained using a general purpose plating bath, Fig. 4, limited the collector efficiency but does not detract from the validity of conclusions about evacuated panels. The black chrome plating process is highly non-linear and any deviation from uniformity in the voltage gradient between the electrodes produces some regions with too thick a coating while others have almost none.

Emissivity was measured using a Devices & Services AE1 emissometer. When testing thin sheet materials there is a tendency for the emissometer to heat the surface, leading to a calibration drift. The effect was minimised by gradually moving the probe head over the surface but this is not infallible for surfaces with non-uniform emissivity. The effect is hard to quantify but an uncertainty of ± 0.03 at each point might be credible.

The reflectivity spectrum was tested for a number of small plating samples and found to vary depending on the coating thickness, Fig. 5. The coating with the lowest emissivity (high infra-red reflectivity) was not completely black and had poor absorptance in the visible and near-IR spectrum. Sample 6F2 has a similar reflectance curve to Lin (from Duffie & Beckman [16]). This testing used a Varian Cary 5000 UV_IR-NIR spectrophotometer which required 50 × 50 mm test pieces; the 470 × 470 mm absorbers could not be evaluated in the same manner. The instrument illuminates the sample with a normal-incidence beam and uses an integrating sphere to capture all the reflected radiation.

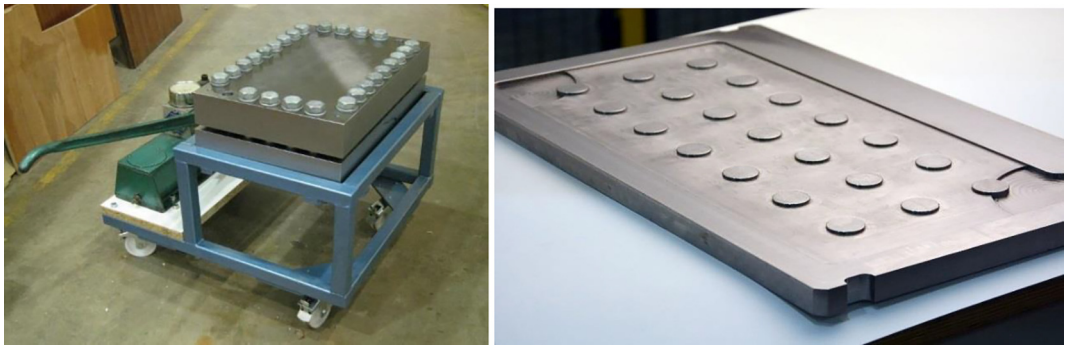

Fig. 2. (a) Hydroforming facility. The clamp plates are 85 mm thick. (b) Mould plate, showing "islands" that generate the dimpled pattern.

2.2. Enclosure manufacture

A number of concepts were initially considered including an all-glass enclosure using glass components bonded with a lead-free "frit" solder glass. The frit's high melting point, typically 450 °C, would however have precluded the use of toughened glass. Concerns about durability when subject to thermal expansion stresses ultimately dictated an alternative approach using low-temperature metal-based solders to bond metal to glass.

Two designs of enclosure were developed, Figs. 6 and 7, for different target applications; each is 0.5 × 0.5 m.

The first design (Henshall, [17]) used a single cover glass over a stainless steel tray. This allowed the pillars to be spot-welded to the tray before sealing the glass in place with a low-temperature solder, Cerasolzer 217. An ultrasonic soldering iron was used to disrupt oxide layers and achieve a satisfactory bond between solder, glass and stainless steel (Arya, [18]).

The second enclosure used two glass panes held apart by a 25 mm deep edge seal to give a symmetrical design. For convenience the pillars were bonded to the lower glass using super-glue prior to soldering the edge seal. When transporting the un-evacuated panel a few pillars came loose. The panel was however tested successfully and the 4 mm toughened glass proved strong enough even when not uniformly supported.

The symmetrical concept could be architecturally attractive as part of a building façade, with the glass visible internally as well as externally. The internal vacuum would then provide thermal insulation for the building in addition to improving the collector efficiency.

The tray collector is a cheaper and lighter alternative for use when the rear side appearance in unimportant, for instance for industrial process heat or in domestic roof-mounted applications. The flexibility of the tray is expected to distribute the air pressure load across the pillars more uniformly than in the symmetrical version. The symmetrical enclosure's pillars sit between two glass sheets that are not completely flat, due to the toughening process; this must cause some maldistribution of stresses since the pillars are nominally all the same length.

The deviation from flatness of a toughened glass sheet is illustrated by the Newton's rings in Fig. 8(a). An untoughened glass pane was placed on top of a sample toughened to BS EN 12150-1. Interference fringes were visible and clearly followed a pair of ridges spaced approximately 36 cm apart. Sliding the upper glass over the lower had little effect on the fringe positions, showing that they were due to the profile of the toughened glass and that the plain glass was sensibly flat by comparison.

This toughened sheet was then placed on a surface table and a dial indicator reading to 1 μm was traversed along two adjacent sides, following axes 50 mm in from the edge (Fig. 8(b)). The two axes intersect close to the $x = 0$ mm position; the end points were 8 mm from the edges of the pane.

The radius of curvature of the glass surface at the right-hand peak on axis 1 was 10 m. Elementary beam theory shows that bending a flat 4 mm sheet to this radius (or flattening a deformed sheet) would result in surface stresses of order 10 MPa. It seems probable that such deviations from flatness would result in significantly increased stresses in the context of an evacuated enclosure with constant length pillars between two glass sheets.

Dial gauge readings for a second toughened sheet showed it have a profile that could be approximated as a spheroid with 16 and 19 m radii of curvature about two perpendicular axes through the centre; the central depth was 2 mm over a 550 mm span. Whilst this may be an extreme case, it highlights the need for careful control of distortion if vacuum enclosures using front and rear glass panes were to be mass-produced.

3. Testing

3.1. Test facility

A dedicated solar simulator was built for the collector efficiency

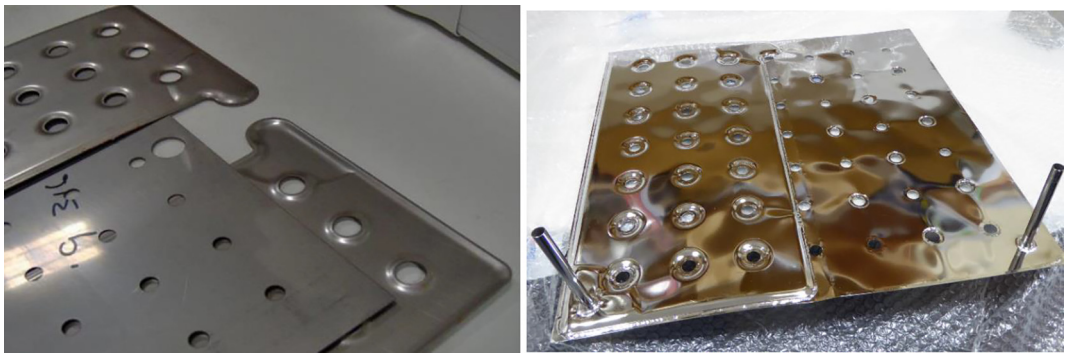

Fig. 3. (a) Laser-cut sheets prior to welding, (b) Absorber after leak testing and electro-polishing, prior to black chrome plating.

65	66	70	n/a	60	58	54	52
53	48	49	57	49	35	28	33
44	46	44	45	36	26	26	25
38	27	38	45	32	23	20	17
35	29	32	44	32	21	15	16
42	29	34	42	32	22	16	16
44	31	35	41	39	24	19	19
n/a	56	60	60	61	54	38	n/a

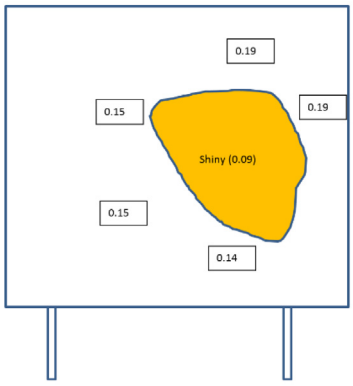

Fig. 4. (a) Emissivity (%) for top surface of the symmetrical absorber, (b) Approximate emissivity of lower surface; the plating of this absorber resulted in very little black chrome on the rear face.

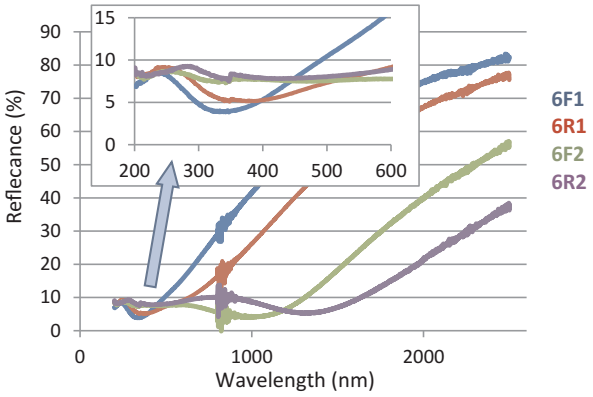

Fig. 5. Reflectivity of four plating samples.

testing, Fig. 9, Moss [19]. This simulator allowed the collectors, instrumentation and vacuum system to remain set up for a period of months without any time constraints or pressure from other users.

The simulator was designed to provide uniform illumination over the panel area: pyranometer measurements over a 5 × 5 grid, Fig. 10(a), demonstrate the uniformity achieved. Four halogen floodlights and an internally reflecting light guide provided multiple virtual images. The light guide is hinged and can be raised to a horizontal position to allow access to the collector.

The visible spectrum was measured using an Eko Instruments LS-100 spectrometer and found to follow a black body curve corresponding to temperatures between 2870 K (1000 W/m^2 using 4 lamps) and 2560 K (100 W/m^2 using 1 lamp), Moss [19]. There was no "cold sky" IR filter and the presence of a long wavelength IR spectral component due to thermal emission from the floodlight cover glasses was inferred from the cover glass temperatures (Moss, [19]). A cooling fan was used to limit the temperature of the collectors' top glass, so the top glass effectively performed as its own IR filter.

Analysis suggests that this long wavelength spectral component has little effect on the collector efficiency measurements providing the cover glass temperature is maintained close to ambient temperature [19]. The heat loss coefficient in an evacuated collector is low because of the high thermal resistance between absorber and cover glass.

A large centrifugal fan blowing across the top cover was used to limit the glass temperature. In the absence of any instrumentation to

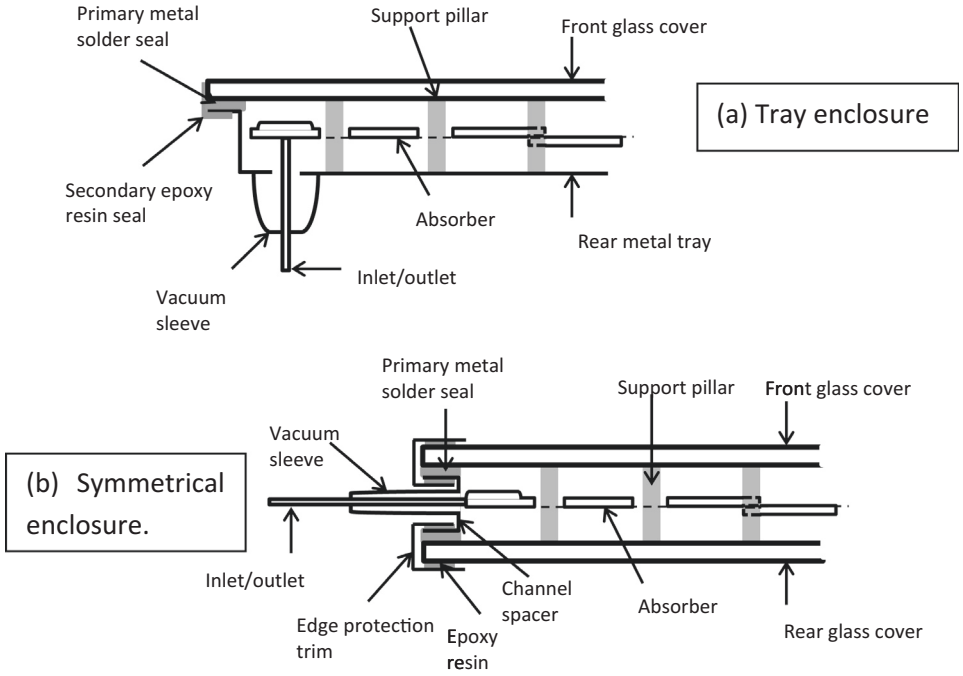

Fig. 6. Cross-sections showing the coolant feed pipe connections, edge seals and pillar geometry: (a) tray enclosure, (b) symmetrical enclosure.

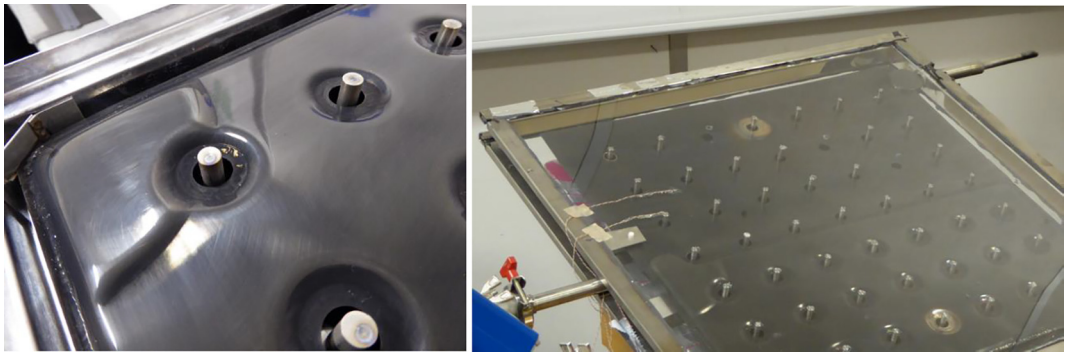

Fig. 7. (a) "Tray" enclosure details showing corner location and deeper absorber section above the feed pipe. (b) The symmetrical collector being instrumented prior to testing.

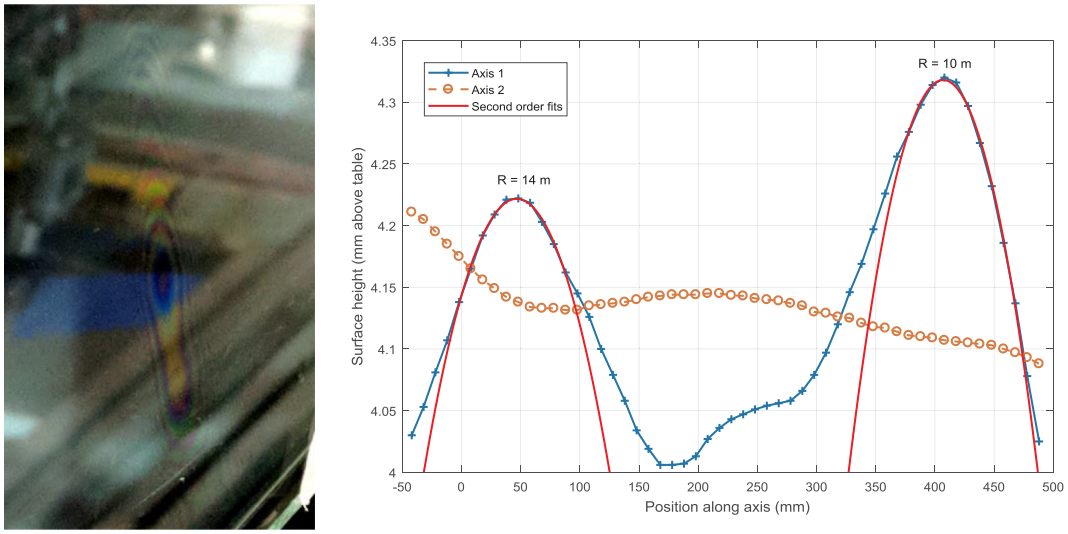

Fig. 8. (a) "Newton's ring" interference fringes showing a contact point between 4 mm toughened and plain glass, (b) Surface profile of this toughened glass sheet.

accurately measure the heat transfer coefficient, wind speed and htc were not measured: instead, the glass was instrumented with thermocouples to measure its temperature directly. The upper glass temperature was typically 12 °C above ambient. Subsequent simulations of the test collectors at $T_M = 50$ °C suggested that under outdoor conditions with $G = 1000\,\mathrm{W/m^2}$ and $h_o = 5.2\,\mathrm{W/m^2\,K}$, the cover glass temperature would rise to 21 °C above ambient. This over-cooling of the top glass will make the measured efficiencies slightly lower than the ideal solar-spectrum efficiencies without a fan [20].

The angular distribution of the illumination could not be measured: a prediction based on the ray-tracing design code is however given in Fig. 10(b). The collectors tested were non-concentrating so the angular distribution should have little effect on the efficiency.

Continuous monitoring of the light output during collector testing was not practicable. A Kipp & Zonen CMP-11 pyranometer was instead used to measure lamp brightness for the range 8–100% of full power. The output was correlated against electrical power (Moss, [19]) in the expectation that this would be more stable than a correlation against voltage.

A repeat measurement 12 weeks later showed the lamp output, at a given power, had risen by 1.5%; a third measurement towards the end of the testing showed the output to be 0.2% below the initial level. For simplicity, the initial calibration was used throughout the efficiency test analysis: this introduces a fractional uncertainty of (−1.5%, +0.2%).

Electrical power was measured using a Hameg HM8115 power meter. Subsequent cross-checking of logbook spot records and the digitised HM8115 output signal suggested that the front panel display was reading 0.66% lower than the output signal. To minimise any possible test to test variations, efficiencies when using two or more lamps have been calculated using the digital signal because it recorded the history of any slight fluctuations during the curve-fit period; for single lamp tests the HM8115's digital output became less credible so log-book values were used. Efficiencies based on the front panel display might be (in fractional terms) 0.66% higher than those presented here. Readers seeking further details are referred to the archived test data set, Moss [20].

3.2. Sensors and accuracy

The coolant flow rate was measured using a Coriolis mass flow meter. Prior to use this was calibrated against a measuring cylinder and stop watch and, within experimental limits, found to be completely accurate. Flow temperatures were measured using Pt100 RTDs and Weissmuller signal conditioning blocks; glass temperatures were measured using type T thermocouples.

IEC60751 Class B RTDs were used. The tolerance on these is ± (0.3 °C + |0.005T|) where T is the temperature in °C i.e. ± 0.7 °C at a coolant temperature of 80 °C. The error in the difference between two temperature readings could on this basis be as high as ± 14 °C. These quoted tolerances however include the effects of manufacturing differences between sensors, random electrical noise and long term drift in the sensors and signal conditioning circuits. The test methodology was designed to cancel out such effects wherever possible.

The accuracy of the experiment depended principally on measurements of the fluid temperature rise as it passed through the absorber. To minimise possible problems due to drift in the absolute temperature

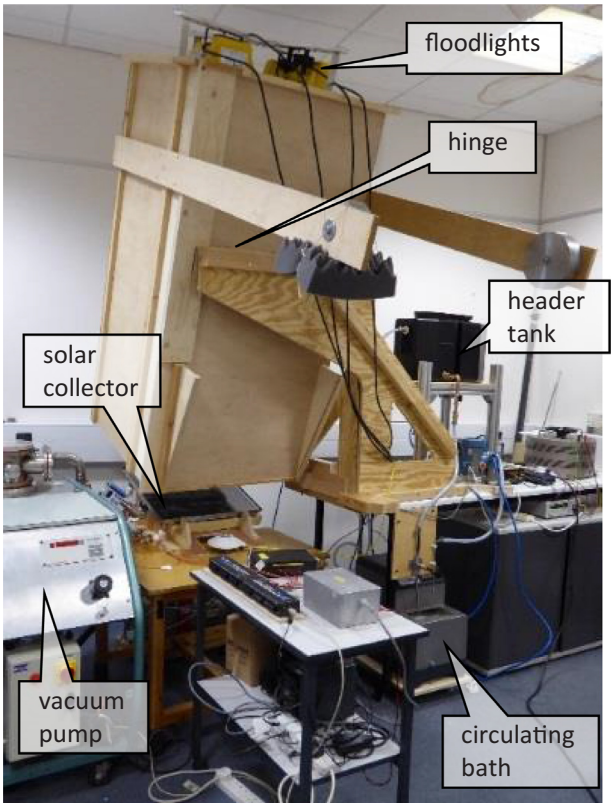

Fig. 9. Simulator and instrumentation during "tray" enclosure testing.

accuracy of the RTDs and thermocouples, prior to each day's testing the enclosure was insulated from the surroundings and coolant was circulated at ambient conditions to obtain a datum temperature reading with zero heat flux. Subsequent datum readings post-test were used to confirm that no zero-shift had occurred during the test period. During each test the flow rate was chosen, at each illumination level, to achieve a large enough temperature rise for accurate measurement, typically in the range 2–7 °C (Moss [20]).

Data was sampled at a rate of 2 Hz using a 16-bit data acquisition system. At each test condition, flow and illumination were held constant until flow temperatures were sufficiently steady (absolute stability is not achievable in practice within a reasonable test period due to the low heat transfer coefficient between absorber and rear glass which lead to a time constant of order 1 h, Moss [20]). After examination to confirm that the signals were of good quality with low noise levels, curve fits were used to obtain a final mean value and minimise any random effects. The curve fit routine provides 95% confidence limits for each coefficient. The median number of fitted points was 600 and the median 95% confidence limit for the heat flux curve fits was ± 0.11%.

The authors know of no simple technique for predicting the expected error after removing initial offsets and noise in this fashion. The efficiency points in Fig. 12 (below) include error bars representing the uncertainty in lamp calibration (−1.5%, +0.2%), electrical power (0.66%) and signal noise (0.11%) which are assumed to act independently. An alternative way of assessing the quality of the data is to examine the variation relative to a linear η versus T_M/G relationship (Section 5). This does not quantify absolute error levels but the closeness of fit to a straight line demonstrates the repeatability of the results.

The most significant source of uncertainty in the efficiency data is likely to be the lack of a completely steady-state operating point in terms of glass temperatures. Hot water from the header tank was passed through the collector for at least 90 min before starting data acquisition; even after this time the rear glass temperature would continue to rise slowly during testing. A shorter time constant could have been achieved by not insulating the rear of the collector but this would have raised concerns about the un-evacuated test giving an unnecessarily poor efficiency.

The low absorber to glass heat transfer coefficients within the evacuated collector are responsible for this long time constant but, conversely, they mean that the effect on the net heat flux to the absorber is small. Predictions suggest that the radiative heat transfer coefficient to the rear glass was of order 1.3 W/m^{2}K. If a typical test achieved $\frac{T_{g,b,ss} - T_{g,b,test}}{T_M} = 0.1$, the apparent heat loss coefficient U_L would be 0.13 W/m^{2}K higher than the steady-state value.

3.3. Test experience

4 mm toughened glass with pillars at 60 mm pitch withstood the 1 bar pressure differential despite the absence of four pillars.

The vacuum pump ran continuously during testing to maintain a sufficiently high vacuum. This was necessary because of out-gassing and leakage through the soldered edge seal.

Vacuum glazing experiments typically seal the evacuated panel after bake-out, under high vacuum conditions (Arya, [18]); having done so, the internal pressure is unknown and the quality of the vacuum can only be inferred from *U*-value measurements. For the current investigation, however, it was desirable to compare efficiency measurements with and without vacuum; for this, the panel needed to be connected to a vacuum system and pressure transducer (JK Lesker combined gauge). Some outgassing is to be expected because, having used low melting point solder to preserve the glass toughness, the assembly cannot be heated to the temperatures in excess of 300 °C that would be required for rapid outgassing (Bacher, [21]).

Over the course of the symmetrical enclosure testing, changes in the pressure achieved by the pump indicated an increase in leakage rate. To

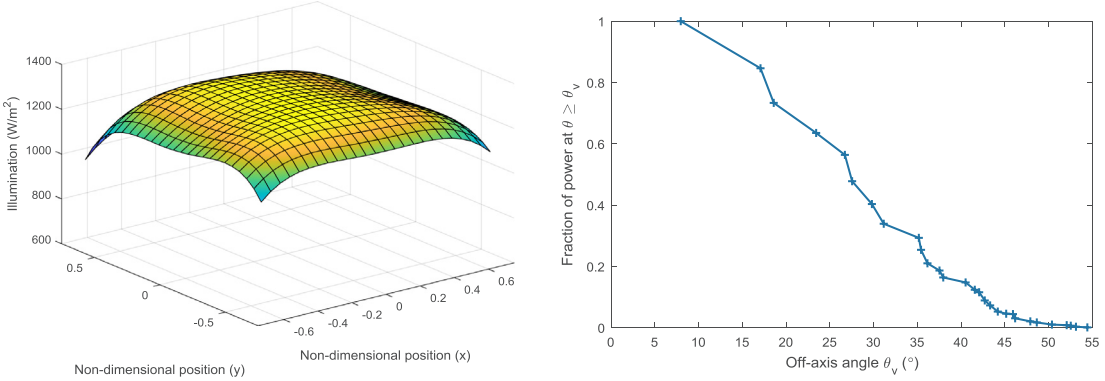

Fig. 10. (a) Polynomial surface fit of pyranometer illumination measurements over a 5 × 5 grid (using all 4 lamps), (b) Predicted cumulative irradiance distribution at the centre of the collector. There is no peak at 0° because the four lamps are arranged symmetrically around the simulator axis; none of them are on-axis.

determine the source of this leakage the enclosure was wrapped in polythene. When helium was introduced inside the bag, the vacuum gauge reading rapidly increased, demonstrating that there was an external leak as opposed to a water leak from the collector. (Helium is useful for identifying high-vacuum leaks: being monatomic it can pass through very small holes). The solder joints were then coated with PermaBond® 382 epoxy which improved the sealing and allowed testing to continue.

It seems likely that the seal degradation resulted from a mismatch in thermal expansion coefficients between glass and the spacer. At the solder solidifying temperature (217 °C), the assembly would be in a stress-free state. Soda-lime glass has an expansion coefficient $8.5 \times 10^{-6}\,K^{-1}$. The spacer was fabricated from 304-grade stainless steel ($\alpha = 17 \times 10^{-6}\,K^{-1}$): at temperatures below 217 °C, the spacer exerts a shear stress on the glass. The simulator raised the cover glass above ambient temperature, exacerbating the problem and increasing the shear stress above the normal room-temperature level.

A microscopic leakage path can cause a significant change in the vacuum level. There was no visual indication of a joint failure and it is unclear whether it occurred within the body of the solder or at the solder/glass interface. The use of 400-grade stainless steel would have provided a better match in terms of expansion coefficients. Shear stresses cannot in practice be completely eliminated by matching expansion coefficients because the temperature difference between the cover glass panes could be as high as 30 °C, e.g. when used as an insulating panel between the inside and outside of a building. Further research is needed into durable vacuum-compatible materials for bonding metal to toughened glass.

4. Results

4.1. Validation of low pressure conduction theory

At high pressures, gas conductivity is independent of pressure; heat is lost from the absorber via conduction, convection and radiation. A moderate reduction in pressure is sufficient to inhibit convection: Eaton and Blum [22] calculated that for a 25 mm plate to glass gap and temperatures of 80 and 20 °C respectively, an internal absolute pressure of 9.3 kPa would be low enough to suppress convection.

A much greater reduction in pressure is required to eliminate the conduction component. Beikircher [23] describes the conductivity of gases at pressures p sufficiently low that the molecular mean free path can exceed the spacing d between surfaces. For a pressure-distance product $pd = 0.00255$ Pa m the effective conductivity is one tenth of the high pressure value. This limit corresponds to a pressure of 0.255 Pa for a 10 mm gap or 0.51 Pa for a 5 mm gap.

Beyond this limit, the heat flux between surfaces is proportional to pressure but independent of the surface spacing. A pressure of 0.051 Pa with a 5 mm gap, for instance, satisfies the pd limit and achieves a 99% reduction in conductive heat flux relative to an ambient pressure case without convection.

Both the current enclosures used 25 mm long pillars. The absorber was approximately 4 mm thick so the mean absorber-glass gap is 10.5 mm. To measure the heat losses, hot water was circulated through the absorber without any illumination, Fig. 11. The enclosure pressure was being reduced using the rotary backing pump. When it reached 4 Pa the pancake valve to the diffusion pump was opened and the pressure fell rapidly, eventually reaching 0.03 Pa. The heat flux from the absorber started to asymptote to the purely radiative level once the pressure was less than 0.5 Pa: this represents a Knudsen number of 1.15, giving a conductivity multiplier of 0.19.

The experiment was not intended to provide a highly accurate validation of the conductivity theory and there will be some uncertainty due to the absorber time constant. It does however prove that an operating pressure of order 0.03 Pa or less is more than adequate to eliminate conduction effects.

4.2. Efficiency data

Both collectors achieved higher efficiencies when evacuated. The tray enclosure efficiency at a nominal operating point of $T_M/G = 0.06$ increased from 36% to 56% when evacuated, Fig. 12(a).

The symmetrical enclosure was tested at more conditions than the tray variant: $T_M = 0$, 20, 31 and 51 °C. In particular having determined the need for a fan to limit the cover glass temperature, enough data points were taken with the fan running to properly illustrate the change in efficiency between evacuated and non-evacuated conditions, Fig. 12(b). These "fan on" efficiency measurements are representative of expected values with solar spectrum illumination in an outdoor context (Moss, [19]) and show the heat loss coefficient reducing from 7.43 to 3.65 W/m^2K when the enclosure is evacuated. This 3.65 value is based on all the evacuated data as opposed to just the $T_M = 51$ °C points in the figure. Moss [20] provides further experimental details.

Efficiency points at high T_M/G conditions were obtained via low illumination powers (down to 128 W/m^2 at $T_M^* = 0.4$ in Fig. 12(b)) rather than high collector temperatures. At low illumination levels the rate of heat loss may exceed the radiation absorbed, giving a negative efficiency. Raising the efficiency by evacuating the enclosure reduces the critical radiation level, below which the collector efficiency becomes negative, in addition to increasing the heat output.

The efficiency definition

$$\eta = \eta_o - \frac{U_L T_M}{G} \tag{2}$$

implies a straight line of gradient $-U_L$ when plotted against T_M/G, if the range of temperatures is small enough that U_L is approximately constant. The straight line fits to the data points in Fig. 12 show this approximation to be valid over the test conditions. The apparent slight difference in high vacuum heat loss coefficient in Fig. 12(b) between water and Tyfocor-LS tests seems unlikely to be a genuine effect; water tests at lower temperatures were closer to the Tyfocor result (Moss [20]).

Defining errors η' relative to two best fit lines (the vacuum and the 1 bar points in Fig. 12, $T_M = 51$ °C) the standard deviation of all η' values is 0.0241. A normal distribution plot, Fig. 13, shows that the distribution of these deviations is approximately normal, with the exception of a few points at the extremes. Taking a 95% confidence interval as ± 1.96 standard deviations from the mean, the uncertainty in each efficiency value may be defined as $1.96 \times 0.0241 = 0.047$. Adding this to the error terms in Section 3.2 gives an efficiency uncertainty $\Delta\eta = [-0.063,\ +0.057]$. These values have been adopted for the error bars in Fig. 12.

The heat loss coefficient U_L should in principle increase slightly with

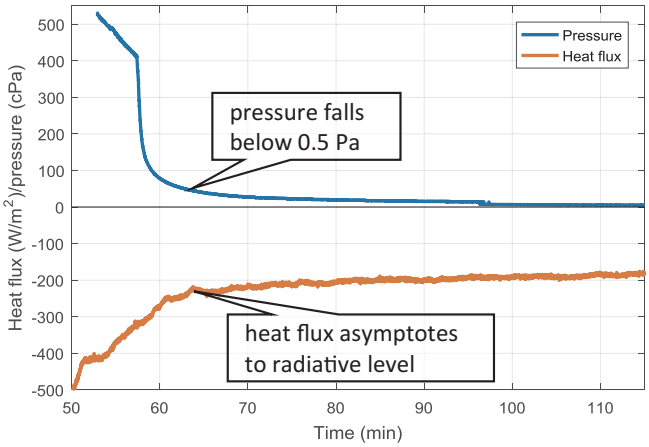

Fig. 11. Reduction in heat losses when the internal pressure was suddenly reduced (tray collector).

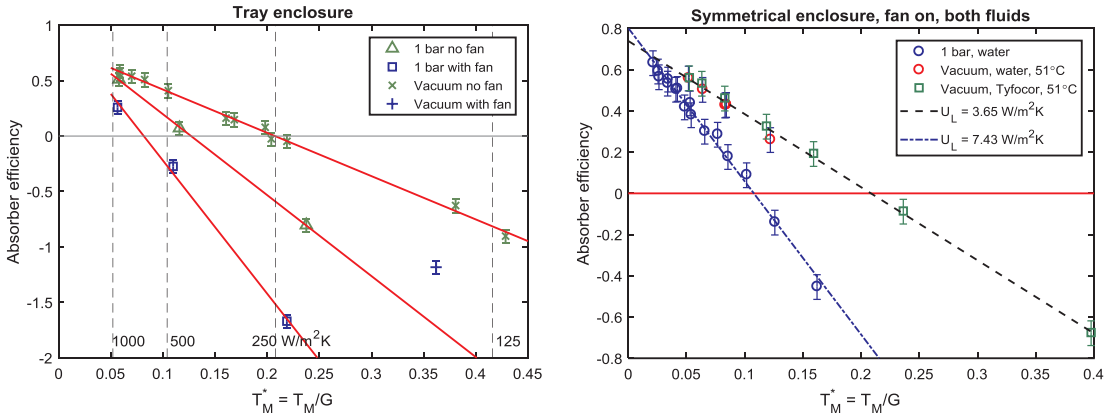

Fig. 12. Test results. (a) Efficiencies for the "tray" enclosure, (b) efficiencies for the symmetrical enclosure.

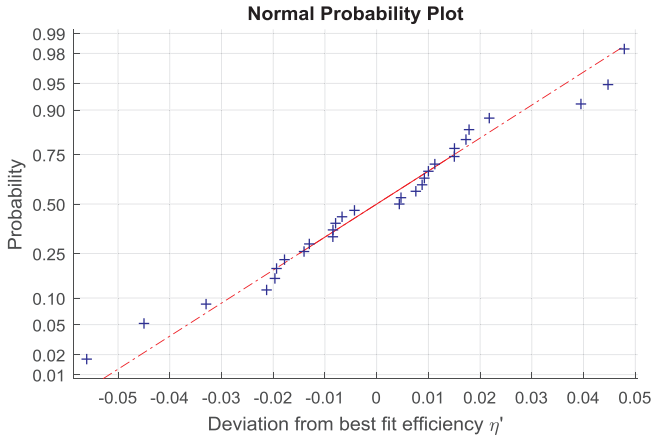

Fig. 13. Distribution of deviations from linear regression lines.

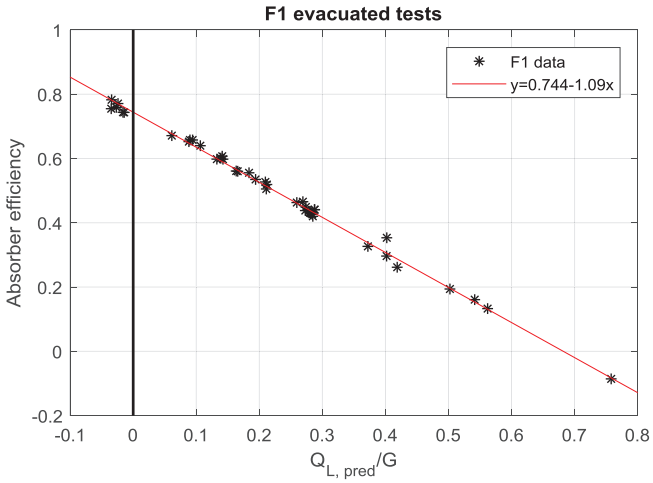

Fig. 14. Comparison of experimental heat loss measurements with an emissivity-based model.

T_M. The best fit lines for the $T_M = 51$ °C points in Fig. 12(b) are:

- 1 bar: $\eta = (0.802 \pm 0.030) - (7.434 \pm 0.417) T_M/G$
- High vacuum: $\eta = (0.7394 \pm 0.019) - (3.547 \pm 0.123) T_M/G$

Whilst not impossible, the optical efficiency (0.802 and 0.739 above) is not expected to vary as a function of pressure. If the optical efficiency were genuinely 0.77, there would be an implied uncertainty in the efficiency data of ± 0.03 to span the 0.74–0.80 range. The reasons for the apparent shift in optical efficiency are unknown: this small uncertainty does not however detract from the overall conclusion that a high vacuum produces a very significant reduction in heat loss coefficient U_L.

The efficiency of the test collectors was limited by the poor selectivity of the black chrome coating. The overall heat loss coefficient was typically 3.65 W/m²K, 9% higher than predicted for the coating emissivity ε = 0.385. Use of a highly selective coating such as Tinox Energy™ with ϵ = 0.04 would give a much lower heat loss coefficient and improved efficiency.

4.3. Radiative heat loss investigation

The test data for the symmetrical enclosure included measurements of the cover glass temperature and the mean absorber temperature could be deduced from inlet and outlet flow temperatures. The radiative heat flux $Q_{L,\ pred}$ between the absorber and the two cover glass panes was predicted from these temperatures using the absorber emissivity measurements and assuming a nominal emissivity of 0.96 for the glass. The absorber-glass gap was much smaller than the absorber width so a parallel plate formula was used without any view factor corrections.

$Q_{L,\ pred}$ is a prediction for $U_L T_M$ and the standard efficiency formula (2) could therefore be rewritten in terms of $Q_{L,\ pred}$ to predict efficiency as $\eta = \eta_o - \frac{Q_{L,pred}}{G}$. A graph of η versus $\frac{Q_{L,pred}}{G}$ (Fig. 14) has a gradient of −1.09 instead of the expected −1, implying that the heat loss coefficient is 9% higher than predicted from the absorber emissivity. This comparison is based on the measured glass temperatures and hence is unaffected by issues such as the IR content in the spectrum or the external heat transfer coefficient; it does however assume that the thermocouple readings are typical of the whole glass surface.

The discrepancy of 9% is no more than might be expected given the difficulty of characterising a thin sheet, unevenly plated absorber using an 8 × 8 grid of spot measurements.

5. Collector modelling and annual output predictions

5.1. Steady state model

A steady-state heat balance simulation (Fig. 15, Table 1) investigated the necessary parameters for matching experimental data from the solar simulator. The algorithm takes a pair of absorber and environment temperatures and solves a quartic heat balance equation to determine the upper and lower cover glass temperatures:

$$-(\varepsilon_{pg,j} + \varepsilon_{eg,j})\sigma T_{g,j}^4 - (h_{i,j} + h_{o,j}) T_{g,j} + (\varepsilon_{pg,j} T_p^4 + \varepsilon_{eg,j} T_{env}^4)\sigma + h_{i,j} T_p + h_{o,j} T_a + q_{abs} = 0$$

where j = 1,2 for the upper and lower surfaces (Moss, [24]).

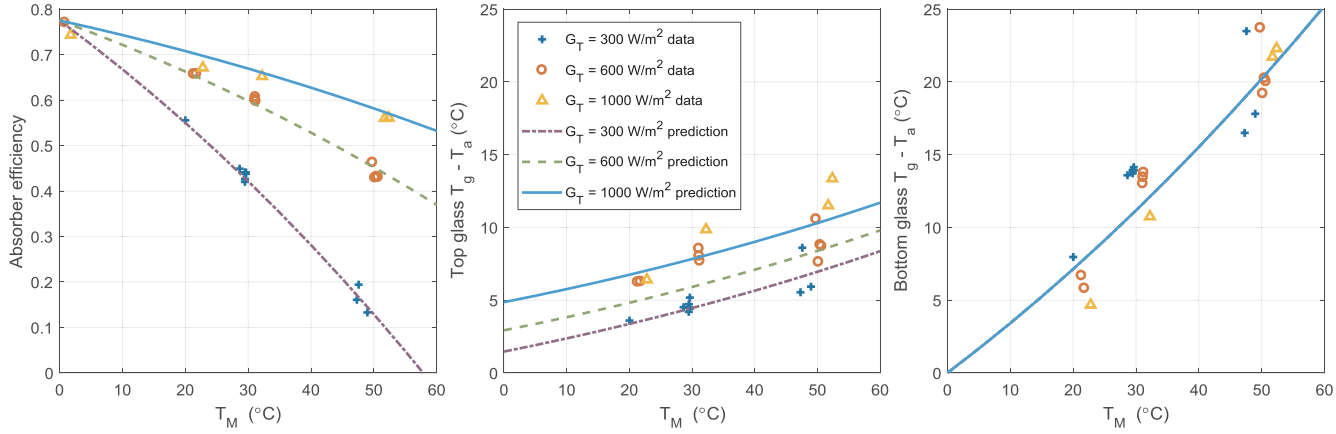

Fig. 15. Comparison of symmetrical enclosure data with simulations (evacuated, fan on); input parameters as Table 1.

Table 1
Comparison of estimated emissivities with best fit values.

	Experiment	Simulation
Upper surface h (W/m² K)	Unknown	22
Absorber top α, ε	unknown, 0.385	0.82, 0.46
Absorber underneathε	0.15	0.15
Lower surface h (W/m² K)	0.44	1.8

Heat transfer within the enclosure was predicted using radiative and low-pressure conduction models; external heat transfer used a given heat transfer coefficient to model the effect of the cooling fan (top) and the insulating support pad (underneath). The glass emissivity was taken as 0.96.

This simulation was in good agreement with the experimental efficiencies and glass temperatures if based on emissivities slightly different to the nominal values, Table 1. Differences relative to the nominal values may reflect the difficulty in taking spot emissivity readings over a surface with considerable non-uniformity; they are also to some extent an artefact of trying to match a transient condition (the lower glass in particular had a long time constant) to a steady-state model.

The simulation code was then run with $\varepsilon = 0.04$ to model the improvement that could be expected with one of the best commercially available selective coatings. The resulting efficiency prediction for an "optimised" EFP is compared in Fig. 16 with the efficiency curves from Fig. 1. The curves have been plotted as a function of irradiance G, assuming normal incidence, at a fixed temperature difference $T_M = 70$ °C.

The parabolic trough (PTC) prediction in Fig. 16 required an expression for the beam fraction f_b (in terms of G) for use in equation [1]. f_b was estimated for every point in the weather data set by comparing G with a clear sky prediction [24]. These f_b estimates were then correlated against G to average the effects of low solar elevation and low f_b, both of which influence G. The derived f_b values for a range of G (dashed lines) are included in the figure. It is not intended to be a highly accurate prediction; instead, it demonstrates that the typically shallow efficiency curve for a concentrating collector (Fig. 1) does not necessarily result in it being the most efficient form of collector at low G.

The "optimised" EFP simulation here predicts a higher efficiency than published data for the SRB panel: this would appear to be simply the result of a more highly selective coating and, without the SRB supporting ribs, a higher fill factor. All the efficiencies decline at low irradiance levels and fall to zero at the critical radiation level. The irradiance distribution (Moss, [24]) has 80% probability of G < 500 W/m² during daylight hours with the Sun in front of the pyranometer. Below this irradiance level the optimised evacuated flat plate has a significantly higher efficiency than conventional collectors.

5.2. Annual output predictions

A simulation of a south-facing collector at an angle of 30° to the horizontal feeding heat into the 85 °C campus heating main at the University of Warwick illustrates the importance of raising panel efficiency. The simulation was based on 6 years of irradiance and air temperature data from the university's weather station, sampled at 1 min intervals. A transient analysis (Moss, [24]) modelled the collector temperature, assuming that the absorber would be held at heating main temperature while producing heat but would cool down (with no circulating flow) whenever there was insufficient irradiance. The university is situated on the outskirts of Coventry and experiences a temperate climate: for periods with the Sun in front of the pyranometer, the annual median irradiance was 172 W/m² and the mean was 279 W/m². The daily mean irradiation at the university weather station, 3.06 kWh/m²/day, is 12% higher than recorded by Palse [25] for Sutton Bonington: at 54 km from Coventry, Sutton Bonington is the nearest Solar Atlas station.

Fig. 17 compares the predicted monthly heat outputs for four collector types in this context. These values represent the mean of the six predicted instances of each month in the 6-year weather dataset.

The estimated f_b values allow Fig. 17 to include a weather data-based prediction for a parabolic trough (PTC); for the other curves they determine the influence of the incidence angle modifier but have no effect on the normal-incidence efficiency. Incidence angle modifiers for the EFP test panels could not be experimentally determined using the

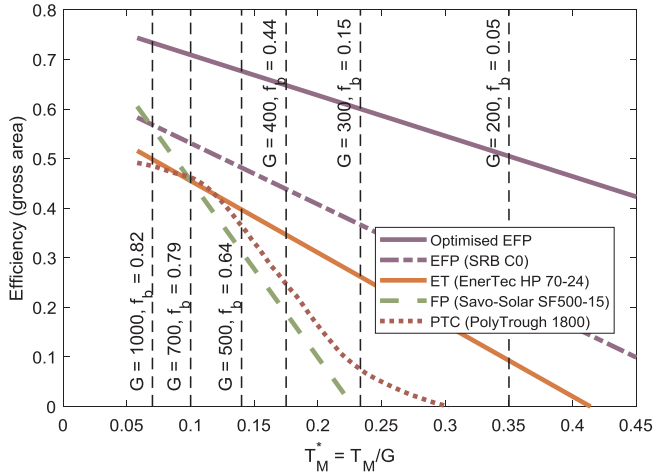

Fig. 16. Simulated normal-incidence efficiency of an optimised evacuated flat plate compared with commercial EFP, evacuated tubes, flat plate and trough collectors operating at $T_M = 70$ °C.

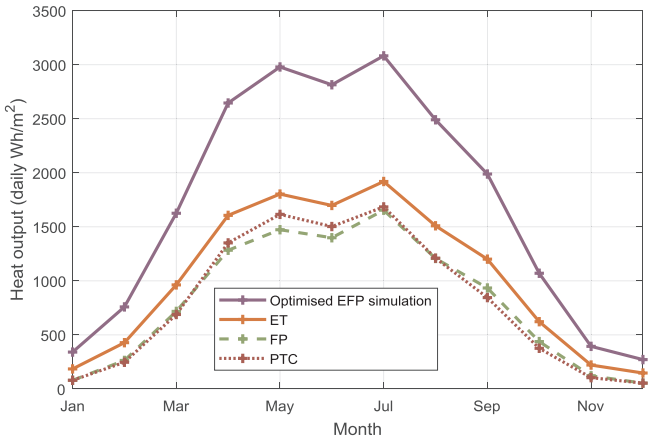

Fig. 17. Predicted heat transfer to an 85 °C district heating main based on weather station irradiance and ambient temperature for 2011–17.

in-house facilities so the EFP simulation adopted a set of conventional flat plate IAM values (SPF data for the Savo-Solar SF500).

The evacuated flat plate simulation generates 66% more heat than the evacuated tube and 112% more than the flat plate; it should be noted moreover that the collectors used for this comparison are amongst the best performers in the SPF database. The benefits of an evacuated flat plate are more evident from such a simulation than from the efficiency curves in Fig. 1.

6. Conclusions

6.1. Design and construction

Previous experimental work on evacuated glazing used indium to seal closely-spaced panes of glass. The current work adopted a cheaper low temperature solder, Cerasolzer 217, applied using an ultrasonically activated soldering iron. The solder sealed well enough to allow high vacuum testing while running a vacuum pump but degradation due to thermal expansion stresses necessitated some re-sealing with epoxy resin. A more durable material would be needed if making 'sealed for life' panels.

Initial problems with glass breakage were overcome by using toughened glass. The combination of 4 mm glass supported by 6 mm diameter pillars at 60 mm pitch proved highly effective and was strong enough to withstand vacuum conditions even with a few pillars missing.

The hydroformed absorber design was chosen after initial work on pressure drop in micro-channels showed that the optimum hydraulic diameter is in the range 2–5 mm and is a function of pumping power. The design worked as expected and would be suitable for mass production using high speed presses and automated laser welding.

6.2. Test conclusions

Both panels demonstrated a significant reduction in heat loss coefficient and a corresponding improvement in efficiency when evacuated to below 0.5 Pa. This pressure limit is as expected from previous work on conduction at low pressures. The heat loss coefficient fell from 7.4 W/m^{2}K to 3.6 W/m^{2}K.

The agreement between test data and a steady-state simulation suggests that all the important heat transfer phenomena are well understood and were correctly modelled.

The efficiency of the test collectors was lower than obtained by the best non-evacuated commercial panels. This is simply because of the relatively high emissivity of the black chrome coatings used on the absorbers here. A simulation based on a higher quality coating indicates that such a panel would provide a very significant efficiency advantage compared to conventional collectors.

6.3. Potential benefits

An evacuated flat panel with a highly selective coating can achieve a significantly higher efficiency than is available from the best conventional flat panels, evacuated tubes or trough collectors. The benefit is most marked at $T_M/G > 0.15$ which in a typical water heating application might equate to $G < 500\,W/m^2$. Weather data suggests this condition is obtained in Coventry for 80% of the annual panel illumination period, so panels with improved efficiency under such conditions could be used to good effect.

A simulation of such a panel connected to the university heating main at 85 °C showed that it would generate an annual heat output 66% higher than the equivalent area of evacuated tubes and 112% higher than from conventional flat plate collectors.

Competing interests statement

The authors have no competing interests.

Acknowledgements

The authors are grateful to the Engineering and Physical Sciences Research Council (EPSRC) for funding this work as part of a collaborative programme between Warwick, Loughborough and Ulster universities, reference EP/K009915/1, EP/K010107/1 and EP/K009230/1. Matlab data and code used for the figures in this paper are openly available from http://wrap.warwick.ac.uk/106468.

Appendix A. Supplementary material

Supplementary data associated with this article can be found, in the online version, at https://doi.org/10.1016/j.tsep.2018.09.003.

References

[1] S. Suman, M.K. Khan, M. Pathak, Performance enhancement of solar collectors – a review, Renew. Sustain. Energy Rev. 49 (2015) 192–210.
[2] N. Benz, T. Beikircher, High efficiency evacuated flat-plate solar collector for process steam production, Solar Energy 65 (2) (1999) 111–118.
[3] T. Beikircher, M. Möckl, P. Osgyan, G. Streib, Advanced solar flat plate collectors with full area absorber, front side film and rear side vacuum superinsulation, Solar Energy Mater. Solar Cells 141 (2015) 308–406.
[4] SPF catalogue of solar collector test results < http://www.spf.ch/index.php?id=111&L=6 > (accessed August 2017).
[5] S. Pauletta, A solar Fresnel collector based on an evacuated flat receiver, Energy Procedia 101 (2016) 480–487, https://doi.org/10.1016/j.egypro.2016.11.061.
[6] F. Buttinger, T. Beikircher, M. Proll, W. Scholkopf, Development of a new flat stationary evacuated CPC-collector for process heat applications, Sol. Energy 84 (2010) 1166–1174.
[7] S. Cohen, G. Grossman, Development of a solar collector with a stationary spherical reflector/tracking absorber for industrial process heat, Sol. Energy 128 (2016) 31–40.
[8] B. Zou, J. Dong, Y. Yao, Y. Jiang, An experimental investigation on a small-sized parabolic trough solar collector for water heating in cold areas, Appl. Energy 163 (2016) 396–407.
[9] J.-L. Bouvier, G. Michaux, P. Salagnac, T. Kientz, D. Rochier, Experimental study of a micro combined heat and power system with a solar parabolic trough collector coupled to a steam Rankine cycle expander, Solar Energy 134 (2016) 180–192.
[10] TVP Solar, MT-30 datasheet, < http://www.tvpsolar.com/files/pagine/1464011780_MT-Power%20Datasheet%20(v4.2x)(ver5).pdf > (accessed 12.07.17).
[11] C. Benvenuti, V. Ruzinov, The SRB evacuated flat solar panel, Proceedings of ECOS 2010, pp. 2-429–434, < https://www.sciencedirect.com/science/journal/03605442/41/1 > .
[12] C. Benvenuti, The SRB solar thermal panel, Europhysics News March 2013, 10.1051/epn/2013301, pp. 16–18.
[13] C. Benvenuti, Particle accelerators and solar panels, Fisica E. 29 (1–2) (2013) 31–38.
[14] R.W. Moss, G.S.F. Shire, P. Henshall, P.C. Eames, F. Arya, T. Hyde, Optimal passage size for solar collector micro-channel and tube-on-plate absorbers, Sol. Energy 153 (2017), https://doi.org/10.1016/j.solener.2017.05.030.

[15] R.W. Moss, G.S.F. Shire, P. Henshall, P.C. Eames, F. Arya, T. Hyde, Design and fabrication of a hydro-formed absorber for an evacuated solar collector, Appl. Therm. Eng. 138 (2018), https://doi.org/10.1016/j.applthermaleng.2018.04.033.
[16] J.A. Duffie, W.A. Beckman, Solar Engineering of Thermal Processes, Figure 4.83, Wiley, 2013 ISBN 9781118418123.
[17] P. Henshall, P. Eames, F. Arya, T. Hyde, R. Moss, S. Shire, Constant temperature induced stresses in evacuated enclosures for high performance flat plate solar thermal collectors, Solar Energy 127 (2016) 250–261.
[18] F. Arya, F. Hyde, P. Henshall, P. Eames, R. Moss, S. Shire, Fabrication and Characterisation of Slim Flat Vacuum Panels Suitable for Solar Applications, EuroSun 2014, Aix-les-Bains, France, September 2014. < http://proceedings.ises.org/paper/eurosun2014/eurosun2014-0045-Arya.pdf > pp. 505–511 (accessed 05.04.18).
[19] R.W. Moss, G.S.F. Shire, P.C. Eames, P. Henshall, T. Hyde, F. Arya, Design and commissioning of a virtual image solar simulator for testing thermal collectors, Sol. Energy 159 (Jan 2018) 234–242, https://doi.org/10.1016/j.solener.2017.10.044.
[20] R.W. Moss, P. Henshall, F. Arya, G.S.F. Shire, P.C. Eames, T. Hyde, Simulator testing of evacuated flat plate solar collectors for industrial heat and building integration, Sol. Energy 164 (April 2018) 109–118, https://doi.org/10.1016/j.solener.2018.02.004.
[21] J.-P. Bacher, C. Benvenuti, P. Chiggiato, M.-P. Reinert, S. Sgobba, A.-M. Brass, Thermal desorption study of selected austenitic stainless steels, J. Vac. Sci. Technol., A 21 (2003) 167, https://doi.org/10.1116/1.1527953.
[22] C.B. Eaton, H.A. Blum, The use of moderate vacuum environments as a means of increasing the collection efficiencies and operating temperatures of flat-plate solar collectors, Sol. Energy 17 (1975) 151–158.
[23] T. Beikircher, G. Goldemund, N. Benz, Gas heat conduction in an evacuated tube solar collector, Sol. Energy 58 (4–6) (1996) 213–217.
[24] R.W. Moss, P. Henshall, F. Arya, G.S.F. Shire, T. Hyde, P.C. Eames, Performance and operational effectiveness of evacuated flat plate solar collectors compared with conventional thermal, PVT and PV panels, Appl. Energy 216 (April 2018) 588–601, https://doi.org/10.1016/j.apenergy.2018.01.001.
[25] W. Palz, J. Grief, European Solar Radiation Atlas, third ed., Springer, 1996.